J Mater Sci (2007) 42:6464–6468
DOI 10.1007/s10853-006-1256-4

Synthesis, structure, and room-temperature ferromagnetism of Ni-doped ZnO nanoparticles

G. J. Huang · J. B. Wang · X. L. Zhong · G. C. Zhou · H. L. Yan

Received: 12 August 2006 / Accepted: 10 November 2006 / Published online: 25 April 2007

Abstract In this paper, Ni-doped ZnO ($Zn_{1-x}Ni_xO$, in which $0 \leq x \leq 0.05$) diluted magnetic semiconductors nanoparticles are prepared by an ultrasonic assisted sol–gel process. Transmission electron microscopy shows sphere-like nanoparticles with an average size of about 25 nm. From the analysis of X-ray diffraction, the Ni-doped ZnO nanoparticles are identified to be a wurtzite structure, but impurity phases are observed when the Ni content x reaches 0.05. Sample structures are further studied by Raman spectra, from which a broad and strong Raman band in the range of 500–600 cm^{-1} is observed in $Zn_{1-x}Ni_xO$. With the increment of x, wurtzite structures degrade gradually. The magnetic properties are measured using superconducting quantum interference device at room temperature; the $Zn_{1-x}Ni_xO$ ($x \leq 0.02$) nanoparticles show ferromagnetism. However, for the sample of $Zn_{0.95}Ni_{0.05}O$, paramagnetism is observed, which may be ascribed to ferromagnetic–antiferromagnetic competition.

Introductions

Zinc oxide (ZnO) has wide range of technological applications as transparent conducting electrodes in solar cells, flat panel displays, surface acoustic wave devices, and sensors. Moreover, it is widely heralded that spintronic devices would provide advantages over their conventional counterparts, such as non-volatility, higher speed, lower power consumption, and higher integration density [1]. Recently, room-temperature (RT) ferromagnetism (FM) in Mn-doped *p*-type ZnO has been predicted by Dietl et al. [2] use a Zener's model. On the other hand, first principles calculations [3] based on density functional theory (DFT) also predict ferromagnetism in most 3*d* transition metal (TM) doped ZnO, which make ZnO one of the most promising material in spintronics, and there is growing interest in this material recently, due to its potential applications in spintronics in which both the spin and the charge of the carriers could be exploited.

At the same time, besides theory predictions, RT FM ZnO doped with TMs has been reported in succession. Among them, most studies focused on Mn-doped ZnO films, while fewer studies on Ni-doped ZnO films have been reported. Liu et al. confirmed the RT FM behavior in their Ni-doped ZnO films synthesized by pulsed laser deposition (PLD) method at room temperature [4]. Magnetic properties of Ni-doped ZnO thin films were also reported [5] for films doped with 3–25 at% Ni, but ferromagnetism could only be observed below 30 K. Besides, Ni^{2+} was successfully doped into ZnO host matrix without forming any secondary phases, however, only paramagnetic behavior was observed [6]. It seems that FM are sensitive to the synthesis conditions, and the origins are still controversial, thus research work in this field is still in its infancy and searching for room RT FM semiconductors which are the foundation for spintronics are still urgency. Moreover, it also seems that most studies focus on film materials, and ferromagnetism could usually only be found in film materials [7].

On the other hand, TM-doped ZnO can be prepared by a variety of methods such as chemical vapor deposition

G. J. Huang · J. B. Wang (✉) · X. L. Zhong · G. C. Zhou · H. L. Yan
Key Laboratory for Low Dimensional Materials & Application Technology of Ministry of Education, Institute of Modern Physics, Xiangtan University, 411105 Xiangtan, Hunan, China
e-mail: jbwang@xtu.edu.cn

(CVD), PLD, and sol–gel process. The CVD and PLD often prove to be too expensive for some industrial applications. The sol–gel process presents some noticeable advantages, such as: a wide possibility of varying the material properties by changing the composition of the starting solution (introduction of dopants and change the material microstructure) [8]; easy to obtain nanoscale materials in volume of gram; and its low costs. Though sol–gel method has been successfully used to synthesis RT FM films [9], no research about the synthesis of RT FM Ni-doped ZnO ($Zn_{1-x}Ni_xO$) nanoparticles has been reported.

In this paper, an ultrasonic assistant sol–gel process is developed to prepare ZnNiO nanoparticles, the structure and magnetism are studied in detail.

Experiment section

$Zn_{1-x}Ni_xO$ nanoparticles are fabricated by a sol–gel process summarized as follows [10, 11]. All the chemicals used here are of analytical grade. First, at room temperature, tetramethylammonium hydroxide ($N(Me)_4OH \cdot 5H_2O$) was dissolved in ethanolic, then a solution (solution A) of 0.55 mol/L was formed; on the other hand, a mixture of $xNi(OAc)_2 \cdot 4H_2O/(1 - x)Zn(OAc)_2 \cdot 2H_2O$ (where $x = 0$, 0.01, 0.02, and 0.05, respectively) were dissolved in DMSO to form another solution (solution B), for which the concentration was 0.10 mol/L. Then, under constant stirring, and with the assistant of ultrasonic, appropriate solution A was added dropwise into the solution B. Resultantly, a sol was formed and dispersed subsequently by ultrasonic. After Ostwald ripening, the sol was iteratively washed by precipitation and resuspension in ethanol so as to remove the excess reactants (Ni^{2+} and Zn^{2+}). The resulting nanocrystals were then capped with dodecylamine. After the solvent being evaporated, the dodecylamine capped nanocrystals were heated in dodecylamine at 200 °C for about 60 min under nitrogen. The resulting powders were then annealed at 500 °C for 30 min under air condition.

JEM-1010 transmission electron microscope (TEM) was used to study the sample morphology and size. The sample structure and composition were carried out by X-ray diffraction (XRD) using a D/MAX 2200 VPC X-ray diffractometer (Rigaku) with Cu-K_α radiation of 1.54056 Å. Raman scattering measurement were performed on a RM2000 micro-laser Raman system at backscattering geometry using the 514.53 nm line of an Ar^+ laser as excitation source. Magnetic measurements were performed on a superconducting quantum interference device (SQUID) magnetometer (MPMS-XL7 Quantum Design, Inc).

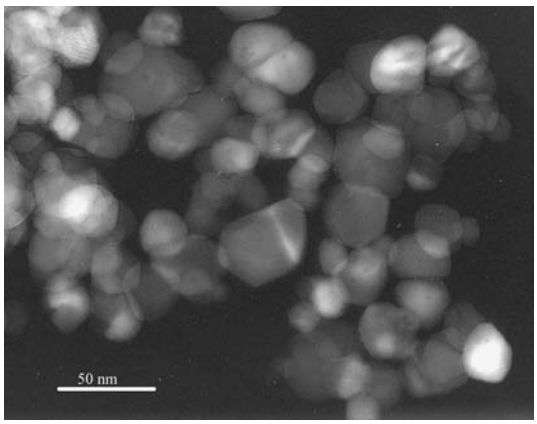

Fig. 1 TEM image of $Zn_{0.99}Ni_{0.01}O$

Results and discussions

Figure 1 shows a typical TEM image (sample $Zn_{0.99}Ni_{0.01}O$) of Ni-doped ZnO nanoparticles, from which the sphere-like morphology could be identified clearly, and the average size of the nanoparticles are estimated to be about 25 nm. The nanoparticles could be dispersed in ethanol easily, which might be the contribution comes from the effect of ultrasonic. As is known that nucleation desorption which is vital to the nanoparticles size could be enhanced by ultrasonic, thus the precursor nucleus could be prevented from overgrown, and the final products could be prone to smaller size.

Powder X-ray diffraction patterns indicate that the as synthesized samples are in a wurtizite structure with all the peaks correspond to ZnO when the content of Ni (x) is less than 0.05, no trace of nickel metal, oxides, or any binary zinc nickel phases is observed (Fig. 2), however, when x reaches 0.05, an additional diffraction peak (identified by arrow in Fig. 2) corresponded to NiO comes into existence,

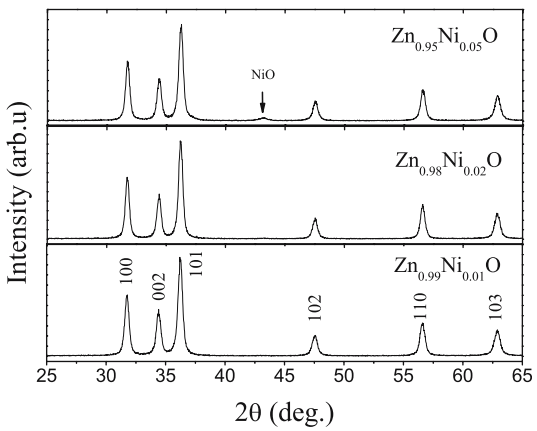

Fig. 2 (**a**) X-ray diffraction patterns of $Zn_{1-x}Ni_xO$ ($x \leq 0.05$) samples

Table 1 The lattice constants calculated from the XRD data of $Zn_{1-x}Ni_xO$ ($0 \leq x \leq 0.05$)

$Zn_{1-x}Ni_xO$			
$x = 0$	$x = 0.01$	$x = 0.02$	$x = 0.05$
a = 3.2404	a = 3.2561	a = 3.2481	a = 3.2526
c = 5.2056	c = 5.2114	c = 5.2164	c = 5.2119

which means that phase segregation has occurred in this system. That's to say, the solubility of Ni in $Zn_{1-x}Ni_xO$ ($x \leq 0.05$) nanoparticles is very low. Higher Ni solubility has been reported in ZnO thin films grown under non-equilibrium conditions such as PLD or rf magnetron sputtering [4, 12]. However, it is obviously much lower in the low-temperature grown samples studied here. Table 1 shows that the lattice constants of $Zn_{1-x}Ni_xO$ ($x > 0$) are slightly larger than those of pure ZnO, because the ionic radius of Ni^{2+} (0.68 Å) is larger than that of Zn^{2+} (0.60 Å). The expansion of the lattice constants of $Zn_{1-x}Ni_xO$ indicated that nickel is really, at least partially, doped into the ZnO structure.

To investigate the influence of Ni doping on microscopic structure and vibrational properties, Raman scattering of the $Zn_{1-x}Ni_xO$ nanoparticles were measured in a backscattering configuration, which is shown in Fig. 3. The Raman-active zone-center optical phonons predicted by the group theory are $A_1 + 2E_2 + E_1$. Both A_1 and E_1 modes are polar and split into transverse optical (TO) and longitudinal optical (LO) phonons. For our $Zn_{1-x}Ni_xO$ nanoparticles, the Raman peaks at 386 cm^{-1} and 582 cm^{-1} could be assigned as A_1 transverse optical (TO) mode (A_1(TO)) and longitudinal optical (LO) mode (A_1(LO)), respectively. The vibrational mode at about 330 cm^{-1} originates from two-phonon process, which is interpreted as $2E_2$(M) by Calleja and Cardona [13]. What is noticeable is the high frequency branch of E_2 mode [E_2 (high)] of ZnO at about 437 cm^{-1},

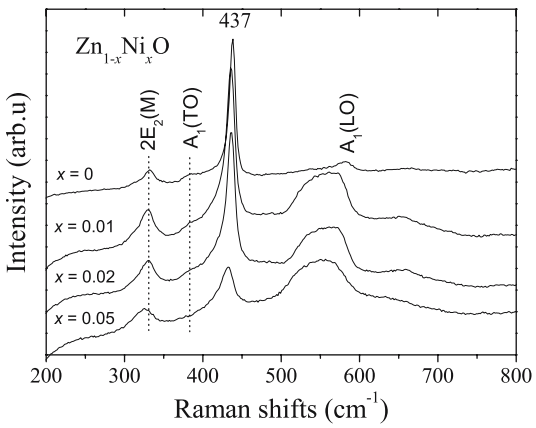

Fig. 3 Raman spectrum for $Zn_{1-x}Ni_xO$ ($0 \leq x \leq 0.05$) samples

for our $Zn_{1-x}Ni_xO$ ($x \leq 0.02$), strong and sharp Raman peaks indicate good wurtzite structures. The sharpest and strongest peak at about 437 cm^{-1} is the strongest Raman mode in wurtzite crystal structure. The value of full width at half maximum (FWHM) of E_2 (high) mode of the samples are less than 11 cm^{-1}, which indicates that $Zn_{1-x}Ni_xO$ ($x \leq 0.02$) nanoparticles keep good ZnO wurtzite structures. However, when the Ni content x increases to 0.05, the Raman line of E_2 (high) mode becomes broad and weak, which means that the wurtzite crystalline structure of ZnO might have been weakened by higher Ni-doping concentration.

Besides the first-order and second-order phonon structure of ZnO, broad and strong band in the range of 500–600 cm^{-1} is observed, which may be due to the density of phonon states (DOPS) of the high-energy phonon branch. It is well known that lattice defects and disorder could usually be introduced by exotic ions doping, defect-induced Raman modes would usually appear in defective crystals because the Raman selection rules are relaxed [14]. For high concentration doped crystal, the translational invariance of the crystal lattice is weakened and scattering events from the whole Brillouin zone are possible, making the DOPS visible. The intensity of the DOPS scales with the doped concentration of ions and, therefore, with the induced crystal damage.

Magnetic properties are studied at room temperature by using SQUID and the results are shown in Fig. 4, from which we can see that, though very weak, clear magnetic hysteresis loops (M–B curves) for both $Zn_{0.99}Ni_{0.01}O$ and $Zn_{0.98}Ni_{0.02}$ are observed (Fig. 4a), which means that the nanoparticles are ferromagnetic with curie temperatures above room temperature. However, the M–B curve (Fig. 4b) of sample $Zn_{0.95}Ni_{0.05}$ shows paramagnetism. The magnetic differences will be discussed in detail later.

The origin of RT FM in transition metal doped ZnO remains an issue of debate. Much work about transition metals doped ZnO focus on Mn-doped ZnO, it is found that conventional superexchange or double-exchange interactions cannot produce long-range magnetic order at concentrations of magnetic cations of a few percent [15]. Several assumptions have been addressed at the moment: the role of the secondary phase, the connection between defects and magnetism, oxygen vacancy, etc. [2, 3, 16–18]. Concerning the origination of RT FM in our $Zn_{1-x}Ni_xO$ ($x \leq 0.02$) samples, we can exclude the possibility that the observed ferromagnetism originates from secondary phase, because: (1) XRD analysis and Raman scattering study have excluded any phase segregation in those $Zn_{1-x}Ni_xO$ ($x \leq 0.02$), which is further confirmed by TEM study; (2) if the observed RT FM really originates from little amount segregations which might not be detected by our XRD or Raman scattering due to their

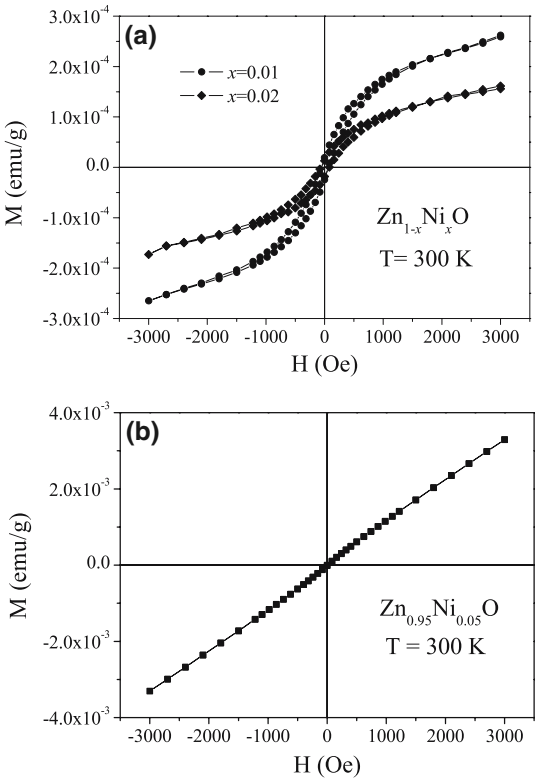

Fig. 4 The magnetic hysteresis loops (M–H curve) of $Zn_{1-x}Ni_xO$ samples: (**a**) $x \leq 0.02$, and (**b**) $x = 0.05$

resolution capacity limitation, then the FM should have been enhanced by increasing Ni contents because segregations should have been increased due to the large driven force for phase segregation [19]. However, as x increasing, the FM decreased; (3) the paramagnetism of $Zn_{0.95}Ni_{0.05}O$ nanoparticles in which NiO impurities are observed is a direct evidence that the ferromagnetism does not originate from secondary phases. Besides, the fact that at higher Ni concentrations, the samples become paramagnetic also can be the evidence that the potential impurities in starting chemicals are not the cause of the observed ferromagnetism at lower Ni content.

Among those models proposed to explain the origination of ferromagnetism in diluted magnetic semiconductors, carrier-mediated ferromagnetism has a possibility as the explanation for the magnetic behaviors observed in this letter. In our $Zn_{1-x}Ni_xO$ ($x \leq 0.02$), abundant defects might have been caused by Ni doping, which could be deduced from Raman spectra [20], which will usually results in n-type ZnO. On the other hand, intrinsic defects such as oxygen vacancies and Zn interstitials, can usually act as shallow donors in ZnO. Therefore, the room-temperature ferromagnetism in $Zn_{1-x}Ni_xO$ ($x \leq 0.02$) nanoparticles could originate from the long-range Ni^{2+}–Ni^{2+} ferromagnetic coupling mediated by shallow donor electrons [15]. Carrier-mediated ferromagnetism in semiconductors is dependent on the magnetic dopant concentration as well as on the carrier type and carrier density. It has been predicted that the higher the n-type carrier doping, the greater the stability of the ferromagnetic phase in ZnNiO. According to Liu et al. [4], as the Ni concentration increases, carrier density decreases due to the compensation of oxygen vacancies, so the ferromagnetism decreases too. On the other hand, as concentration increases, Ni atoms can come close to each other, which implies the presence of some Ni^{2+} ions with Ni^{2+} nearest neighbors. The superexchange interactions between these neighboring Ni^{2+} ions are antiferromagnetic. Increasing Ni concentration will increase the volume fraction of Ni^{2+} ions with Ni^{2+} nearest neighbors. As a result, the enhanced antiferromagnetic interaction suppresses ferromagnetic coupling. Besides, when Ni^{2+} content x reaches 0.05, NiO, which contributes antiferromagnetism is formed, so the ferromagnetism in ZnNiO system is suppressed, and then, a large paramagnetism effect is observed.

Conclusion

In summary, Ni-doped ZnO ($Zn_{1-x}Ni_xO$, $0 \leq x \leq 0.05$) diluted magnetic semiconductors nanoparticles are prepared by an ultrasonic assisted sol–gel process. XRD analysis and Raman study show wurtzite structures for all the $Zn_{1-x}Ni_xO$ nanoparticles. With increasing Ni concentration, the wurtzite structures degrade gradually. Clear magnetic hysteresis loops indicates FM are observed in $Zn_{1-x}Ni_xO$ ($x \leq 0.02$) system, and the Curie temperature is higher than 300 K. It is probable that the RT FM might originate from long-range Ni^{2+}–Ni^{2+} ferromagnetic coupling mediated by shallow donor electrons. However, when x increasing to 0.05, antiferromagnetic NiO formed and the system turns to be paramagnetic.

Acknowledgements This work was financially supported by the Hunan Provincial Natural Science Foundation of China (No. 05JJ30126), the Scientific Research Fund of Hunan Provincial Education Department (No. 04B061), the Key Laboratory of Low Dimensional Materials & Application Technology (Xiangtan University), Ministry of Education (No. KF0506), and the Fund of Xiangtan University (05IND10).

Referrences

1. Jeong YH, Han S-J, Park J-H, Lee YH (2004) J Magn Magn Mater 272–276:1976
2. Dietl T, Ohno H, Matsukura F, Cibert J, Ferrand D (2000) Science 287:1019
3. Sluiter MHF, Kawazoe Y, Sharma P, Inoue A, Raju AR, Rout C, Waghmare UV (2005) Phys Rev Lett 94:187204

4. Liu XX, Lin FT, Sun LL, Cheng WJ, Ma XM, Shi WZ (2006) Appl Phys Lett 88:062508
5. Wakano T, Fujimura N, Morinaga Y, Abe N, Ashida A, Ito T (2001) Physica C 10:260
6. Yin Z, Chen N, Yang F, Song S, Chai C, Zhong J, Qian H, Ibrahim K (2005) Solid State Commun 135:430
7. Coey JMD (2005) J Appl Phys 97:10D313
8. Martinez AI, Acosta DR (2005) Thin Solid Films 483:107
9. Kima YM, Yoona M, Parka I-W, Parkb YJ, Lyou JH (2004) Solid State Commun 129:175
10. Norberg NS, Kittilstved KR, Amonette JE, Kukkadapu RK, Schwartz DA, Gamelin DR (2004) J Am Chem Soc 126:9387
11. Schwartz DA, Norberg NS, Nguyen QP, Parker JM, Gamelin DR (2003) J Am Chem Soc 125:13205
12. Yin Z, Chen N, Yang F, Song S, Chai C, Zhong J, Qian H, Ibrahim K (2005) Solid State Commun 135:430
13. Calleja JM, Cardona M (1977) Phys Rev B 16:3753
14. Chartier A, Arco PD, Dovesi R, Saunders VR (1999) Phys Rev B 60:14042
15. Coey JMD, Venkatesan M, Fitzgerald CB (2005) Nat Mater 4:173
16. Pearton SJ, Norton DP, Ip K, Heo YW, Steiner T (2005) Progr Mater Sci 50:293
17. Venkatesan M, Fitzgerald CB, Coey JMD (2004) Nature 430:630
18. Eriksson O, Bergqvist L, Sanyal B, Kudnovsky J, Drchal V, Korzhavyi P, Turek I (2004) J Phys Condens Matter 16:S5481
19. Jayaram V, Rani BS (2001) Mater Sci Eng A 304:800
20. Wang JB, Huang GJ, Zhong XL, Sun LZ, Zhou YC, Liu EH (2006) Appl Phys Lett 88:252502